JACS Au
AN OPEN ACCESS JOURNAL OF THE AMERICAN CHEMICAL SOCIETY

pubs.acs.org/jacsau
Article

Taming Conformational Heterogeneity on Ion Racetrack to Unveil Principles that Drive Membrane Permeation of Cyclosporines

Miranda N. Limbach, Edward T. Lindberg, Hernando J. Olivos, Lara van Tetering, Carlos A. Steren, Jonathan Martens, Van A. Ngo, Jos Oomens, and Thanh D. Do*

Cite This: *JACS Au* 2024, 4, 1458−1470

ABSTRACT: Our study reveals the underlying principles governing the passive membrane permeability in three large *N*-methylated macrocyclic peptides (*N*-MeMPs): cyclosporine A (CycA), Alisporivir (ALI), and cyclosporine H (CycH). We determine a series of conformers required for robust passive membrane diffusion and those relevant to other functions, such as binding to protein targets or intermediates, in the presence of solvent additives. We investigate the conformational interconversions and establish correlations with the membrane permeability. Nuclear magnetic resonance (NMR) and cyclic ion-mobility spectrometry-mass spectrometry (cIMS-MS) are employed to characterize conformational heterogeneity and identify *cis*-amides relevant for good membrane permeability. In addition, ion mobility selected cIMS-MS and infrared (IR) multiple-photon dissociation (IRMPD) spectroscopy experiments are conducted to evaluate the energy barriers between conformations. We observe that CycA and ALI, both cyclosporines with favorable membrane permeabilities, display multiple stable and well-defined conformers. In contrast, CycH, an epimer of CycA with limited permeability, exhibits fewer and fewer stable conformers. We demonstrate the essential role of the conformational shift from the aqueous *cis* MeVal11−MeBmt1 state (**A1**) to the closed conformation featuring *cis* MeLeu9−MeLeu10 (**C1**) in facilitating membrane permeation. Additionally, we highlight that the transition from **A1** to the all-*trans* open conformation (**O1**) is specifically triggered by the presence of $CaCl_2$. We also capture a set of conformers with *cis* Sar3−MeLeu4, MeLeu9−MeLeu10, denoted as **I**. Conformationally selected cIMS-MS and IRMPD data of $[CycA+Ca]^{2+}$ show immediate repopulation of the original population distribution, suggesting that $CaCl_2$ smooths out the energy barriers. Finally, our work presents an improved sampling molecular dynamics approach based on a refined force field that not only consistently and accurately captures established conformers of cyclosporines but also exhibits strong predictive capabilities for novel conformers.

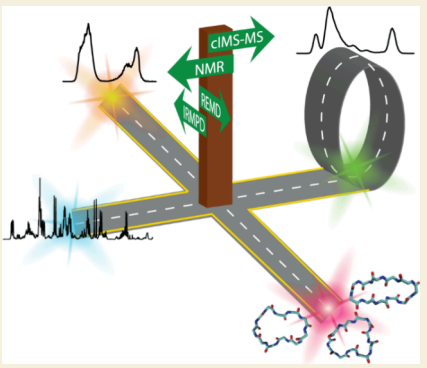

KEYWORDS: *Cyclosporine, cyclic ion mobility spectrometry, nuclear magnetic resonance, molecular dynamics, conformational heterogeneity, membrane permeability*

INTRODUCTION

The precise regulation of interactions between peptides and cellular membranes holds significant potential for unlocking a broad range of innovative applications including cargo delivery, tissue labeling, cellular imaging, and therapeutic intervention. Within this realm, *N*-methylated macrocyclic peptides (*N*-MeMPs) have emerged as a class of cyclic compounds exhibiting promising medicinal properties. Since their molecular weights (MW) are 600 Da or higher, their chemical actions are not confined by Lipinski's rule of 5, which describes traditional therapeutics with a molecular mass of less than 500 Da, no more than 5 hydrogen bond donors, no more than 10 hydrogen bond acceptors, and an octanol−water partition coefficient not greater than 5.[1−3] Their biochemical and therapeutic attributes are expected to fill the gap in chemical space between small molecules and linear peptides.[4−8]

Approximately 75% of disease-relevant proteins involved in intracellular protein−protein interfaces (PPIs) are considered "undruggable" by small molecules.[9−11] Cyclosporine A (CycA), an 11-residue cyclic peptide that binds at the interface between cyclophilin A (CypA) and two calcineurins, illustrates a clear example that macrocyclic compounds, including *N*-MeMPs, can potentially address this disparity.

A significant hurdle remains: most existing, and notably the most exciting, *N*-MeMP drugs (e.g., CycA) originate from natural products, and we appear to be unable to design new drugs that work similarly to CycA. The relatively limited deployment of cyclic peptide medicinal agents thus far has resulted from the lack of strategies to design membrane-

Received: January 3, 2024
Revised: March 5, 2024
Accepted: March 5, 2024
Published: March 16, 2024

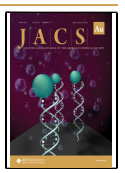

https://doi.org/10.1021/jacsau.4c00011
JACS Au 2024, 4, 1458−1470

permeable cyclic peptides. Membrane permeability is a critical property that is essential for any drug to target intracellular proteins. Consequently, over the past two decades, only 18 cyclic peptides have been approved for clinical use, with only two that target intracellular proteins (Romidepsin and Voclosporin).[12−14] This starkly contrasts the approval of 32 small-molecule drugs in 2021[13] and 16 in 2022.[15] None of the recently approved small-molecule drugs target PPIs or could potentially replace cyclic peptide drugs such as CycA and Voclosporin (a synthetic cyclosporine). Therefore, a comprehensive understanding of the factors that control the membrane permeability of *N*-MeMPs is crucial to address the bottleneck in the drug design and will unlock their unique pharmaceutical novelty.

CycA, with a primary sequence of cyclo(MeBmt1—Abu2—Sar3—MeLeu4—Val5—MeLeu6—Ala7—D-Ala8—MeLeu9—MeLeu10—MeVal11), revolutionized the field of organ transplants.[16−18] CycA contains seven *N*-methylated residues, several consecutive, implying that up to seven amide bonds can adopt *cis* or *trans* configurations. Mathematically, this results in up to 2^7 = 128 possible conformers solely classified based on backbone *cis/trans* configurations. This number is substantial, especially when contrasted with fewer than a handful of available high-resolution structures. Within the cyclosporine family, one structural modification, such as (de)methylation or stereoinversion, can drastically alter the structures, biological target(s), and membrane permeability.[19−23]

The same cyclosporine can bind to distinct protein targets with unique bound states. For example, CycA binds at the interface between CypA and calcineurins to exert its immunosuppressant property[24−26] with a conformer with all-*trans* amides (**O1**) and also binds to the Regulator Gene of Glucosyltransferase (**RGG**) in *Streptococcus* to exhibit its inhibitory effect with a conformer that has three *cis*-amides.[27] This is intriguing because it goes against the traditional model in protein−ligand theory, which assumes rigid ligands and flexible protein active sites. In contrast, cyclosporines exhibit enough flexibility to adjust their conformation to fit the groove-shaped binding sites.

Before the report of the aqueous conformer of CycA,[28] the closed (**C1**) form[29] with a *cis* MeLeu9−MeLeu10 in apolar solvents and the open (**O1**) form in the protein complex[24−26] formed the basis for the passive membrane permeability hypothesis, where **C1** is thought to exist in the membrane environment, and **O1** exists in aqueous solution.[19,30] This hypothesis and limitations in high-resolution structural data have resulted in contradictory structure−function data. For instance, cyclosporines exhibiting comparable biological activities, such as CycA and cyclosporine G (CycG),[31,32] were erroneously believed to assume different conformations.[20] It is noteworthy that both CycA and CycG primarily adopt the **A1** conformation in solution, but while **A1** of CycG was documented in 2003,[33] that of CycA[28] was only reported two decades later (in 2022).

The presence of diverse conformations is the enabling factor for the unique and diverse functions of cyclosporines. However, we have yet to understand the extent of this conformational space and the potential links between various conformation states (or structural dynamics, the interconversion among these conformers) and the functional roles.

This work establishes the key principles that drive membrane permeation in the cyclosporine family. The relationship between conformational heterogeneity, isomerism, and passive membrane diffusion of cyclic peptides has not yet been fully understood. Evidently, analogues stabilizing either **O1** or **C1** failed to achieve the desired membrane permeability and affinity to CypA.[19,21,34] The membrane permeability of cyclosporines is likely dictated by interconversions among a set of conformers (aqueous, membrane-bound, and intermediates in between) rather than individual conformers.[30] The problem at hand is to identify precisely what all possible conformers are and how the environments can stabilize each of them and thus their permeabilities. To validate this hypothesis, this work (a) investigates cyclosporine analogues, chosen due to their differences in membrane permeability, and (b) synergizes a collection of bioanalytical techniques for a robust sampling of cyclosporine conformational space.

In particular, we chose to work with **CycA**, Alisporivir (**ALI**), and cyclosporine H (**CycH**). ALI is a synthetic nonimmunosuppressant analogue, developed by Debiopharm, that has comparable membrane permeability to CycA and also binds strongly to CypA.[35,36] ALI was strategically designed for differing from CycA at only two residues, D-MeAla3 and EtVal4, so it does not bind calcineurin.[34,37,38] ALI is currently being researched for potential use in treating hepatitis C[35,39,40] and SARS-CoV-2.[41] The second analogue, CycH, is a CycA epimer with a D-MeVal11. The biochemical properties of CycA and CycH are drastically different. The most notable ones are CycH's poor membrane permeability and weak affinity to CypA.[34] A summary of the macrocycle residue alterations with respect to CycA and their physiochemical properties is provided in Figure 1.

This work uses a combination of solution two-dimensional nuclear magnetic resonance (2D-NMR), three ion-mobility platforms; drift-tube, cyclic, and trapped ion mobility spectrometry (DT-IMS, cIMS, and TIMS, respectively), and ion spectroscopy (IR multiple-photon dissociation; IRMPD) coupled with TIMS and Fourier-transform ion cyclotron

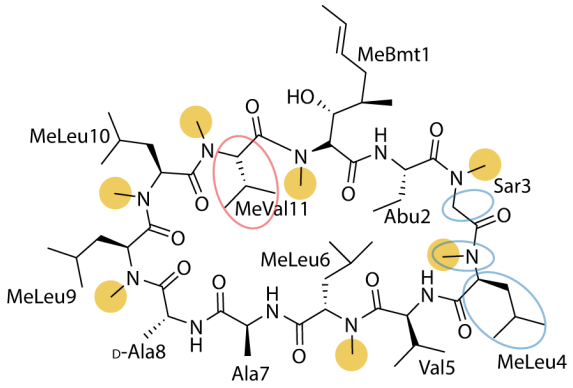

Compd Name	Residue Alterations	Membrane Permeability	Binding Affinity
CycA	n/a	Good	Strong
ALI	D-MeAla3 EtVal4	Good	Strong
CycH	D-MeVal11	Poor	Weak

Figure 1. Chemical structure of CycA. A summary of residue alterations with respect to CycA is provided in the table as well as illustrated in blue for ALI and red for CycH. The seven *N*-methylated amides are also highlighted in yellow. The cellular permeability and relative binding affinity to CypA are also provided.

https://doi.org/10.1021/jacsau.4c00011
JACS Au 2024, 4, 1458−1470

resonance (FT-ICR). The ultimate goal is to comprehensively capture major and minor cyclosporine conformers in aqueous environments, their interconversion, and their responses to external perturbation (temperature or ionic salts). With 2D-NMR, conformers are classified based on their *cis/trans* amide configurations and chemical shifts. Direct exchange between conformers with different *cis/trans* configurations has not been observed in 2D-NMR because the typical activation energy for *cis/trans* isomerization in linear molecules is approximately 20 kcal/mol,[42,43] which is equivalent to transition times on the order of minutes. IMS offers a longer time scale than NMR, and ion activation on mobility-selected conformers provides unique information about interconversion.[44] IRMPD provides spectroscopic signatures of the molecule and its conformers in the mass spectrometer. Finally, we will present a molecular dynamics (MD) approach based on a reparameterized force field, specific for cyclosporines, to enhance conformational sampling and improve predictive power.

Notably, pairing multiple complementary techniques in analyzing biomolecules has not been the standard practice for the structural analysis of cyclic peptides in general and cyclosporines in particular. Our work herein describes a thorough sampling of cyclosporine conformers, illuminating the critical roles of "redundant" *N*-methylation in cyclosporines in their biochemical functions. We also highlight new approaches to predict the membrane permeability of cyclosporine-based analogues.

MATERIALS AND METHODS

NMR Spectroscopy

Sample preparation, instrumentation, and software details can be found in the Materials and Methods section of the Supporting Information. 2D-NMR experiments are vital for atomically resolving the conformers and obtaining chemical exchange information between states. 2D through-bond NMR experiments zTOCSY (Total Correlation Spectroscopy), ^{13}C-gHSQC (Heteronuclear Single Quantum Coherence) with adiabatic pulses, and ^{13}C-gHMBC (Heteronuclear Multiple Bond Correlation) with adiabatic pulses are used to identify each amino acid residue and assign the protons and carbons within them. Then, ROESY (Rotating Frame Overhauser Enhancement Spectroscopy) with adiabatic pulses (ROESYAD, also known as easy ROESY) is a through-space experiment that indicates protons that are in close spatial proximity ($\lesssim$5 Å). This experiment is used to connect the residues in sequence and identify the *cis/trans* amide connections. The distance restraints from ROESY experiments can be used to construct a structural model in NMR molecular dynamics simulations. Additionally, the ROESY cross peaks (ROEs) in the same phase as the diagonal indicate nuclei in chemical exchange on the NMR time scale (approximately 300 ms).

Ion Mobility Spectrometry-Mass Spectrometry

All sample preparation, instrumentation, and software details can be found in the Materials and Methods section of the Supporting Information. DT-IMS-MS experiments were conducted to evaluate the mass spectra, collisional cross sections (CCS), and arrival time distributions (ATDs) of the conformers. DT-IMS instrument parameters are listed in Table S1.

cIMS-MS experiments were conducted to obtain high-resolution ion mobility chromatographic information. The multipass capabilities of cIMS-MS allow for increased separation of conformers compared to DT-IMS. Conformations can then be mobility-selected and reintroduced into the cyclic ion racetrack for additional passes, which provide further separation and conformational interconversion insights. Instrument parameters are listed in Table S2.

IR Multiple-Photon Dissociation Spectroscopy

Sample preparation, instrumentation, and software details can be found in the Materials and Methods section of the Supporting Information and Table S3. IRMPD spectroscopy is a powerful technique used to probe an ion's vibrational modes and, by extension, the structure.[45−47] We verify the gas-phase conformational structures selected by IMS-MS. The setup is based on Fourier-transform ion cyclotron resonance (FTICR)-MS (Bruker SolariX) with an electrospray ionization (ESI) source and a trapped ion mobility spectrometry (TIMS) stage. In the ICR cell, the *m*/*z*- and IMS-selected ions are irradiated with the pulsed, tunable laser light from FELIX so that IRMPD spectra are obtained. The experimental IR spectra are compared with DFT-predicted IR spectra to make conformation assignments.

Computational Modeling

Temperature-based replica exchange molecular dynamics (T-REMD) simulations were performed in an explicit methanol solvent box for CycA, ALI, and CycH. The parameters for the macrocyclic solute molecules were generated from a modified ff14SB AMBER force field.[48] For charge derivation, we have employed the PyRED server[49] to perform a restrained electrostatic potential fit for the atomic charge values using four separate conformations of CycA, two of which are from the RCSB Protein Data Bank and the other from our NMR/X-ray/neutron crystallography data.[50−53] Four dipeptide fragments (Abu2—Sar3, Val5—MeLeu6, MeLeu9—MeLeu10, and MeVal11—MeBmt1) were used for charge derivation in addition to three single amino acid fragments (MeLeu4, Ala7, and D-Ala8). The four amino acid pairs in CycA's X-ray structures show significant experimental *cis* propensity. Therefore, we accordingly estimated the contribution from torsion of the peptide bond as 0 kcal/mol. In doing so, we assume that the energetic contribution from other sources is more relevant in conformer selection. The simulations are 2.5 μs/replica. Simulation convergence was assessed by block analysis and correlation matrices (Figures S1 and S2). The conformers were further geometry optimized for energy calculations with Density Functional Theory (DFT). Additional details on the REMD simulation parameters and DFT calculations (Figure S3) can be found in the Supporting Information.

RESULTS

NMR Spectroscopy of CycA, ALI, and CycH

An illustration of the NMR-observed *cis*-amide backbone connections in CycA, ALI, and CycH is shown in Scheme 1. The circles indicate the residues connected by a methylated amide bond and are filled in with black if a *cis* configuration has been observed via our NMR data. The red and blue dashed lines denote additional structures containing both *cis*-amides. The conformational heterogeneity of the three cyclosporines is investigated by 2D-NMR spectroscopy (Tables S4 and S15 for ^{1}H and ^{13}C assigned chemical shifts). *Cis*-amide bonds are followed and assigned in the Hα-Hα region of the ROESY spectra. Conformers are defined as structures with unique *cis/trans* amide backbones. States are denoted as the conformer letter followed by an integer, with "1" being the most abundant state, e.g., **A1** and **A2** refer to two states of the "aqueous" conformer, both containing the *cis* MeVal11—MeBmt1. We recall that "states" are defined as various forms of the same conformer, which have identical *cis/trans* amide backbone conformations and are assumed to have similar structures. States are often observed in slow exchange on the NMR time scale. This nomenclature was used in our previous work.[28]

All three compounds (CycA, ALI, and CycH) adopt **C1**. We previously showed that CycA populated **A1** and **C1** as the major conformers. In addition, there are minor conformers of CycA with *cis*-amides Abu2—Sar3 and Val5—MeLeu6 that we

https://doi.org/10.1021/jacsau.4c00011
JACS Au 2024, 4, 1458−1470

Scheme 1. Peptide Backbone Connection Scheme of CycA, ALI, and CycH Based on NMR Data[a]

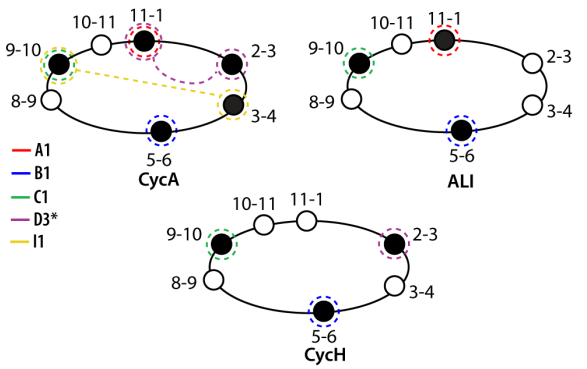

[a]Circles indicate residues that are connected by a methylated amide. Black circles denote an NMR-observed *cis*-amide. Each color represents a unique conformer. *Cis*-amides that are connected are found in the same conformer. The all-*trans* conformers were observed for all three macrocycles. D-Ala8—MeLeu9 and MeLeu10—MeVal11 are always *trans*. **D3** is partial.

termed **D1**−**3**.[28] Here, our NMR data reveal that **O1** and **A1** are prominent conformers for ALI, while **C1** and **B1** (a *cis* Val5-MeLeu6 conformer) are minor conformers (partially assigned). CycH was found to adopt **C1** and **O1** as major conformers, which is in agreement with CycH's X-ray crystal structures.[33] CycH also adopts **B1** as a major conformer and a partially assigned *cis* Abu2—Sar3 as a minor conformer. Intriguingly, while both CycA and ALI populate **A1**, CycH does not (Figure 2A). Of note, we verify that the conformers observed in the NMR experiments have the same *cis*-amide bonds and the same hydrogen bonds as the X-ray crystal structures (see Tables S16−S21).

Additionally, the chemical exchange between states can be assessed by signals in the HN-HN region of the ROESY spectra with the same phase as that on the diagonal (Figure 2B). Counting the exchange peaks, CycA and ALI exhibit at least 15 exchanges among states, while CycH exhibits at least 21. The CycA and ALI exchange signals are strong, while the CycH spectrum is more congested with poorly defined peaks, resulting in overlapping signals and making atomic assignment difficult (Figure 2C).

NMR Spectroscopy of CycA+Ca^{2+}

We and others previously performed 2D-NMR experiments of CycA in the presence of $CaCl_2$, where we found that the population of **O1** significantly increased.[54] However, previous studies did not thoroughly investigate other changes in solution, especially the abundance of **A1** and the formation of any new conformer. Here, we repeat the experiments and carefully monitor the changes in the samples over 2 weeks. An equilibrated ensemble is attained after 2 weeks (see Figure S4). Further investigation of the equilibrated sample reveals two main observations, as elaborated below.

First, the population of **C1** is relatively unaffected, but **A1** is decreased, and **O1** is increased (Figure 3A). This is consistent with our previous report.[54] Second, the evolution of a new signal becomes apparent at temperatures greater than 25 °C (Figure 3B). Analysis of the TOCSY spectrum identifies this signal as the Hα of a MeLeu6. This signal was traced in the ROESY spectrum to reveal that it belongs to a conformer with a *cis* Sar3—MeLeu4 and MeLeu9—MeLeu10 backbone configuration (Figure 3C), which we have denoted as **I2**. We referred to this conformer as **I2** because Bernardi and co-workers previously reported another conformer with the same *cis*-amides.[55] Henceforth, we designate the conformer identified by Bernardi as **I***, the conformer anticipated by T-REMD (without salt) as **I1**, and the novel conformer observed in the presence of $CaCl_2$ as **I2** (refer to Table S19 for hydrogen bond calculations related to **I2**).

IMS-MS of CycA, ALI, and CycH

The conformational ensembles of the macrocycles are further investigated with DT-IMS (Figure S5) and multipass cIMS-MS. The mass-selected IMS mobiligram of $[CycA+H]^+$ in

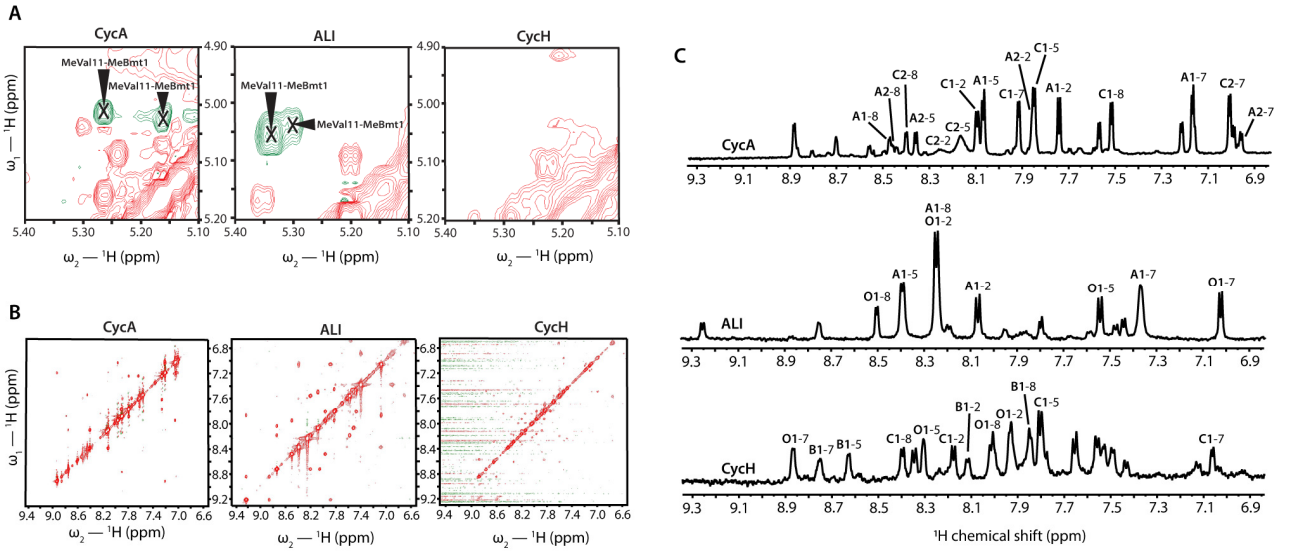

Figure 2. (A) MeVal11(Hα)− MeBmt1(Hα) ROESY cross peaks (ROEs) of **A1** and **A2**, indicating the *cis*-amides. The ROEs are found for CycA and ALI, but they are absent for CycH. (B) ROESY spectrum showing exchange peaks (in red) between states. (C) The NH-NH region of the ^{1}H NMR spectrum of CycA, ALI, and CycH is shown in panel C. All spectra were taken at 25 °C. The samples are 5 mM in CD_3OD with 10% H_2O.

https://doi.org/10.1021/jacsau.4c00011
JACS Au 2024, 4, 1458−1470

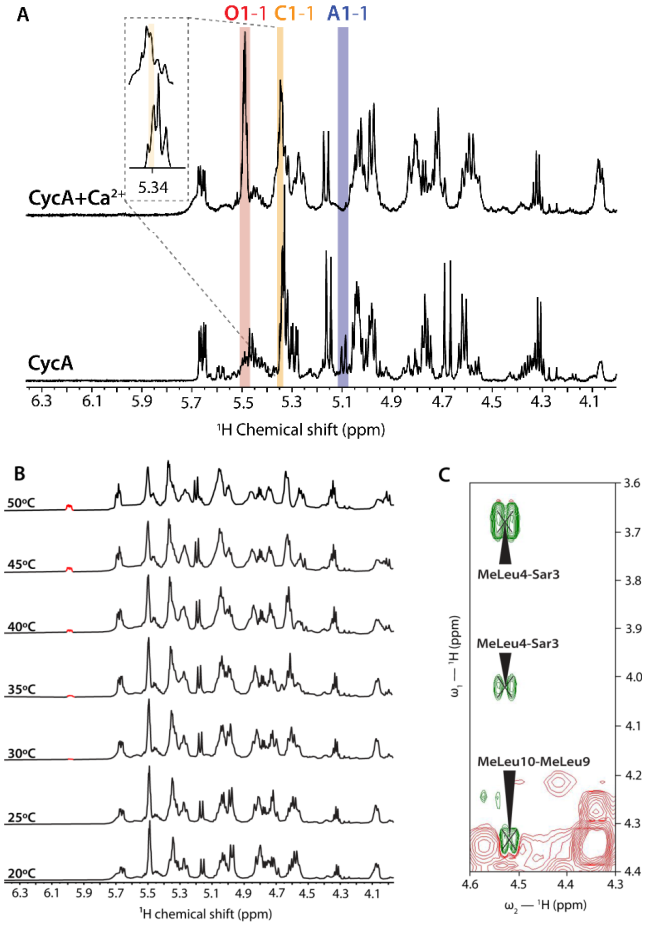

Figure 3. (A) Hα-Hα ^{1}H NMR region of 5 mM CycA samples in CD_3CN with approximately 0.7% H_2O with and without 5 mM calcium chloride at 25 °C. Proton signals of MeBmt1 are annotated for each conformer. (B) Partial ^{1}H NMR spectra of CycA:$CaCl_2$ sample at various temperatures. The signal highlighted in light purple is the Hα of MeLeu6 of **I2**. (B) Hα-Hα ROEs of the 2 *cis*-amides found of **I2**. Two MeLeu4-Sar3 ROEs were observed because Sar3 has two Hα's.

Figure 4 shows four major features (similar to the data of ALI as seen in Figure S6) after 10 passes on the cyclic ion racetrack. CycH, on the other hand, shows only two features after 9 passes.

For CycA, mobility-selecting the most compact or extended conformers and reintroducing them into the cyclic path does not re-establish the initial conformational ensemble. Partial re-equilibration is observed at 60 eV (lab frame) when ion activation is used. Nonetheless, even at 80 eV, the initial distributions of four IM features are not established, indicating a high energy barrier between the compact and extended conformers. A similar result is obtained for the ALI (Figure S6).

On the other hand, when each IM feature of $[CycH+H]^+$ was separately introduced to the ion racetrack, the original conformers were repopulating after only about four passes without ion activation (Figure 4B). This is evident by the almost immediate overlapping of the mobility-selected conformer baselines. The repopulation of the two distinct conformers can be seen after 8 additional passes. Population distributions do not change much after increasing the energy to 80 eV.

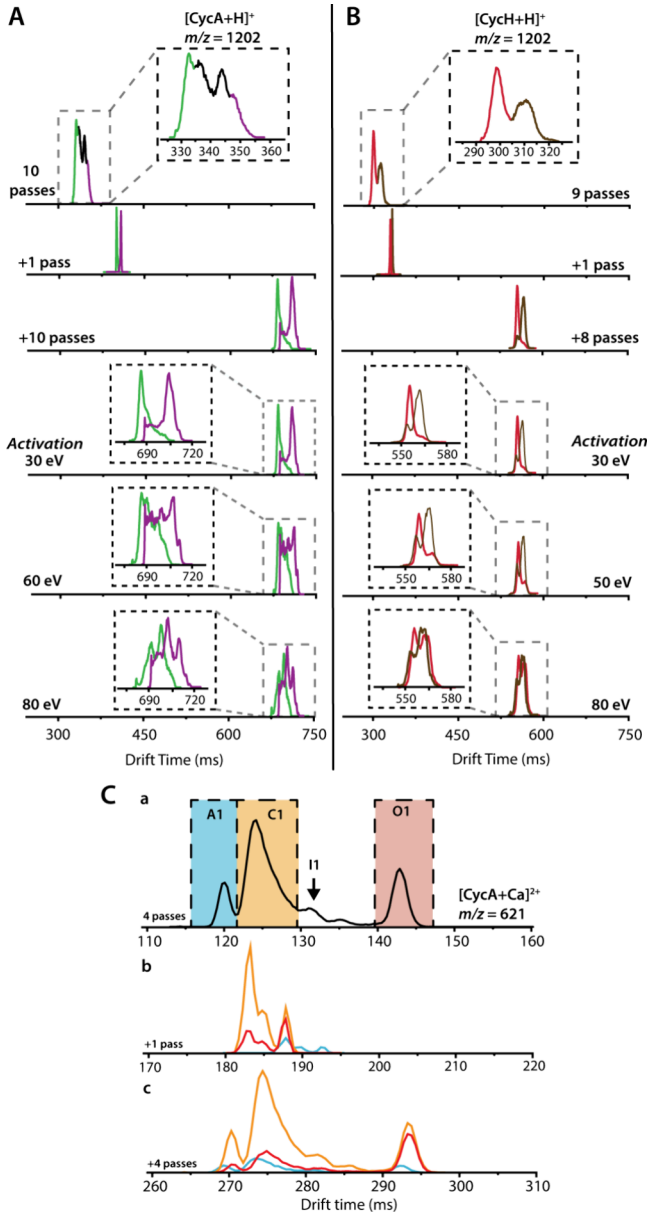

Figure 4. cIMS-MS data for singly protonated (A) CycA and (B) CycH. The IM profile of CycA after 10 passes contains four major features, whereas that of CycH after 9 passes contains only two features. Mobility-selecting conformers with either the shortest or the longest drift times (green or purple features of $[CycA+H]^+$; red or brown features of $[CycH+H]^+$) yields partial distributions of the initial ensembles without the addition of ion activation. With ion activation energy, the two distinct conformers of CycH can be re-established from either conformer, while this is not the case for CycA. (C) cIMS-MS data of the doubly charged calciated adduct of CycA, $[CycA+Ca]^{2+}$. The conformational ensemble without ion mobility selection is shown in panel a. cIMS-MS data on mobility-selected conformers (**A1**-cyan, **C1**-orange, **O1**-red) are shown in panels b and c. Initial distribution is re-established starting from any of the three conformers without ion activation. **I1** was tentatively assigned based on the theoretical CCS calculations, which indicates that **I1** is slightly larger than **C1**, and is significantly smaller than **O1**.

IMS-MS of CycA in the Presence of Ca^{2+}

When comparing the DT-IMS-MS data of $[CycA+H]^+$ and $[CycA+Ca]^{2+}$ and making assignments based on the relative differences in CCS among the major conformers (**A1** < **C1** <

https://doi.org/10.1021/jacsau.4c00011
JACS Au 2024, 4, 1458−1470

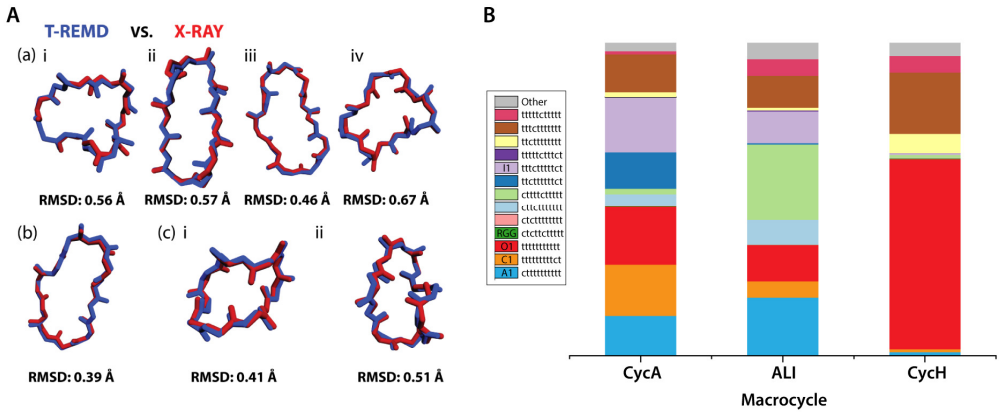

Figure 5. Data from ~2 μs of T-REMD simulations. (A) Backbone RMSD comparison of T-REMD (blue) with X-ray structures (red) for CycA (i-iv are **A1**, **C1**, **O1**, and **RGG** of CycA, respectively), ALI (**O1**), and CycH (i and ii are **O1** and **C1** of CycH, respectively), indicating the accuracy of our T-REMD to sample each experimentally observed conformation. (B) The *cis/trans* isomer distribution of CycA, ALI, and CycH sampled by the simulation. Convergence of the simulation was assessed by using the relative entropy of blocked conformer distributions.

O1; see Table S23 for experimental and theoretical CCS), the data suggest that the population of **O1** increases significantly, while that of **A1** decreases in the presence of $CaCl_2$. With cIMS-MS, we can reproduce this result with a better resolution (Figure 4C; and see Figure S8 for $[CycH+Ca]^{2+}$ and $[ALI+Ca]^{2+}$ data). Lastly, the IM feature assigned to **C1** is broad and tailing toward the longer drift time, indicating some minor conformers between **C1** and **O1**. Given this, one could argue that Ca^{2+} binds initially to **A1**, facilitating **A1** to **O1** conversion.

However, if that mechanism were correct, we would expect that Ca^{2+} selectively perturbed the transition from **A1** to **O1** but not from **A1** to **C1** or from **C1** to **O1**. Ion activation experiments with cIMS-MS indicate that the conformational transitions among all CycA conformers are more fluid in the presence of Ca^{2+}. Recall that the same experiments on singly protonated CycA revealed that it was impossible to re-establish the conformational ensemble starting with either the most compact or most extended conformers, even with an 80 eV activation voltage. On the other hand, with $[CycA+Ca]^{2+}$, the introduction of any of the Ca^{2+} bound conformers to the ion racetrack quickly establishes the original ensemble without the addition of activation voltage (Figure 4C, panels b and c).

Computational Modeling of CycA, ALI, and CycH

With the modified force field, our T-REMD data capture all of the experimentally detected CycA, ALI, and CycH conformers reported. Namely, with CycA, these include the X-ray crystal structures of **A1**,[28] **C1**,[56] **O1**,[24] and also **RGG** (the conformer with three *cis*-amides that binds to the RGG protein[27]), the **C1**[57] and **O1**[33] of the free CycH, and **O1** of ALI,[37] see Figure 5.

For CycA, conformational heterogeneity is much higher in the simulation data (no conformer occupies more than 25% of the total population) that those obtained by Ono et al. (in methanol, Ono et al. predicted the all-*trans* conformer to be ~50%).[58] This result also shows a better agreement with our NMR data than that of Ono et al.[58] For ALI, the only reported X-ray crystal structure is its all-*trans* open form in the CypA:ALI complex, which the simulations captured. More importantly, the T-REMD results of ALI and CycH are not biased toward the known structures of CycA, for which the X-ray structures were used to parametrize the force field. This indicates that our force field provides a fair assessment of the cyclosporines.

T-REMD data validate our NMR and IMS-MS findings. Specifically, the data highlight that CycH is much less heterogeneous than CycA and ALI. CycH's **O1** is the predominant conformer, whereas in CycA and ALI, the two competing conformers are **A1** and **C1**, or **A1** and **O1**, respectively.

The predictive capabilities inherent in our T-REMD data are strong. Notably, while there is a preference toward conformers with no or one *cis*-amides, the computational results also indicate the presence of conformers with more than one *cis* bond. For example, the Pearson correlation matrixes of *cis/trans* methylated amides (Figure S2) indicate the strong propensity for the coexistence of Abu2—Sar3, Val5—MeLeu6, and MeVal11—MeBmt1 (found in the RGG-bound conformer), or Sar3—MeLeu4 and MeLeu9—MeLeu10. Interestingly, the conformer with *cis* Sar3—MeLeu4 and MeLeu9—MeLeu10 (i.e., "**I1**"). Conformers with the same *cis*-amides have previously been reported in the NMR experiment of CycA in the presence of $Mg(ClO_4)_2$ by Bernardi and coworkers;[55] however, there might be variations in backbone structures). Our T-REMD experiments predict that the **I** conformers are among the relevant conformers of CycA. We will discuss **I1** and its variants (**I*** and **I2**) in more detail in the next section.

Regarding ALI, T-REMD data reinforce that the chemical modification stabilizes **O1** but does not impair **A1**. The change of Sar3 to D-MeAla3 lowers the *cis* propensity of the amide between residues 2 and 3, while the change of MeLeu4 to EtVal4 has the same effect on the amide between residues 3 and 4. In parallel, T-REMD predicts that in addition to **A1** and **O1**, ALI should populate a conformer with two *cis*-amides Val5—MeLeu6 and MeVal11—MeBmt1. This result is reasonable because the chemical modifications at residues 3 and 4 in ALI strategically stabilize the *trans* configurations at the amides among residues 2, 3, and 4. Thus, this conformer shares a similar *cis/trans* configuration to CycA's **RGG,** except for the lack of *cis*-amide between Abu2 and Sar3. A *cis* Val5—MeLeu6 conformer was previously observed in NMR experiments for CycA (denoted as **D3** in Limbach et al.[28]) and presently observed in ALI, but the conformer was partially resolved.

https://doi.org/10.1021/jacsau.4c00011
JACS Au 2024, 4, 1458−1470

In summary, the T-REMD simulations capture the experimental conformers observed in NMR and X-ray crystallography and predict the existence of conformers with more than one *cis* bond that may play essential roles in conformational transitions among the major conformers.

Ion Mobility-Selected IR Multiple-Photon Dissociation Spectroscopy

To verify the identity of the gas-phase $[CycA+Ca]^{2+}$ conformers beyond the CCS from the IMS-MS data, IRMPD spectroscopy is employed with and without TIMS selection. The TIMS mobilogram of $[CycA+Ca]^{2+}$ (Figure 6A) is similar to the ATD of the same species obtained using cIMS-MS (Figure 4) and DT-IMS.[54] A notable difference is the intensity of peak **I1**, which becomes intense in the TIMS mobilogram.

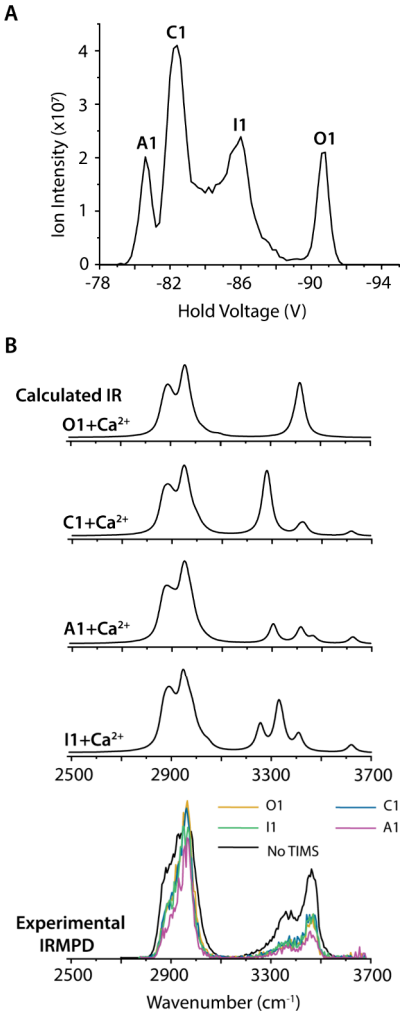

Figure 6. (A) TIMS mobiligram of $[CycA+Ca]^{2+}$. Four features are observed and are annotated as **A1**, **C1**, **I1**, and **O1**. (B) DFT-calculated IR spectra of $[CycA+Ca]^{2+}$'s **O1**, **C1**, **A1**, and **I1** with Ca^{2+} obtained from DFT calculations and compared to experimental IRMPD spectra of $[CycA+Ca]^{2+}$ when mobility-selecting the peaks corresponding to **A1**, **C1**, **I1**, and **O1** (orange, dark blue, green, purple, respectively) and without TIMS (black). The C−H stretching frequency (2500−3000 cm^{-1}) and the O−H/N-H stretching frequency range (3000−3700 cm^{-1}) are shown. A scaling factor of 0.950 was applied to the computed harmonic frequencies to account for the anharmonicity.

DFT-calculated IR spectra of CycA's **O1**, **C1**, **A1**, and **I1** in the presence of Ca^{2+} obtained from DFT calculations are compared with the experimental IRMPD spectrum of $[CycA+Ca]^{2+}$ (Figure 6B). The IRMPD spectrum shows a shouldered band in the C−H stretching region and two distinct bands in the O−H and N−H stretching ranges, which are attributed to MeBmt1 and to nonmethylated amides, respectively.

We also recorded TIMS-mobility selected IRMPD spectra for each peak observed in the TIMS mobilogram.[59] The IRMPD spectra of peaks assigned to **C1** and **O1**, respectively are almost identical, while that of **A1** has a small difference in the band intensities. We posit that when a calciated conformer is mobility-selected in the TIMS, it quickly re-equilibrates into a conformational ensemble, either upon extraction from the TIMS and storage in the ICR cell or upon IR excitation. The rationale is consistent with our cIMS-MS data on mobility-selected ions shown in Figure 4C and discussed above. Note that the observation that there are discernible structures in the cIMS and TIMS data is not in conflict with our statement that re-equilibration may happen upon extraction from the TIMS, residence in the ICR cell, or upon IR multiple-photon excitation (MPE).

DISCUSSION

Conformational Heterogeneity, Especially the Presence of Closed and Aqueous Conformers, Is Critical for Good Membrane Permeability

Conformational heterogeneity is commonly regarded as an unfavorable characteristic of a ligand in protein−ligand interactions. However, it is an inherent outcome of *N*-methylation in cyclic peptides. The presence of conformational heterogeneity and flexibility contradicts the notion of cyclization, which aims to reduce the conformational space in the molecule. Here, our work helps rationalize the ability of cyclosporines to cross membranes and rearrange to bind protein targets.

All three compounds (CycA, ALI, and CycH) adopt **C1**. Among them, the hydrogen bonding patterns differ slightly in each macrocycle. According to our MD simulations, ALI cannot form the Abu2-NH···Val5-CO hydrogen bond, possibly because of the backbone strain from the D-amino acid at position 3, with the added methyl group replacing a hydrogen that normally eclipses the adjacent *N*-methylation. CycH does not form the two hydrogen bonds involving residues 7 and 8, presumably due to epimer-induced backbone strain. Of note, despite these differences, each macrocycle forms the β-turn between residues 3 and 4 and successfully shields their amide hydrogens from solvent. This is clear evidence that a closed conformer alone does not indicate good membrane permeability. This is consistent with early work on cyclosporine O (CycO), which stabilizes the closed form but has poor membrane permeability.[21]

Our previous NMR study showed that **O1** is a minor population of CycA that becomes populated in the presence of $CaCl_2$ (more discussion to follow).[54] Here, our NMR data reveal that **O1** is a prominent conformer in ALI. Since both CycA and ALI are good membrane-permeable peptides,[35,37,41] we conclude that the abundance of **O1** (or generally, a conformer with all-*trans* amides) does not predict membrane permeability. Regarding **O1**, while this conformer of CycA and ALI are very similar (as both molecules bind tightly to

https://doi.org/10.1021/jacsau.4c00011
JACS Au 2024, 4, 1458−1470

CypA[24,25,37]), that of CycH (which does not bind strongly to CypA[34]) is different. The characteristic transannular hydrogen bond of **O1** in CycA is that between the side chain hydroxyl of MeBmt1 and MeLeu4's carbonyl oxygen. According to X-ray structures and DFT and MD calculations, this hydrogen bond persists in ALI despite the substitution on residue 4. However, CycH's epimerization introduces enough ring strain to entirely prohibit this hydrogen bond, preferring a hydrogen bond between MeBmt1's side chain oxygen and Abu2's carbonyl oxygen instead.

Lastly, both CycA and ALI, the two macrocycles with good membrane permeability, populate **A1**, while CycH, which has poor membrane permeability, does not (Figure 2A). The L to D isomerization of MeVal11 disrupts the ability of the MeVal11—MeBmt1 amide bond to adopt the *cis* configuration. The **A1** conformer in CycA was previously probed via NMR and crystallography techniques, and its relevance to CycA biochemistry was discussed in detail.[28] Cyclosporines that eliminate *cis* MeVal11—MeBmt1 via demethylation of MeVal11, such as cyclosporine E (CycE)[20] and some analogues of CycO,[60] also have poor membrane permeability. Collectively, the presence of **A1** in membrane-permeable CycA, ALI, and CycG (see ref.[33]) suggests that this conformer is critical for the macrocycles to diffuse across the lipid bilayer passively.

Beyond individual conformers, we envisage, based on the NMR data alone, that the number of exchanges among states is inversely proportional to conformational heterogeneity. CycA and ALI's NMR spectra show fewer exchanges but strong peaks, indicating fewer exchanges among states with the same *cis*−*trans* configurations. On the other hand, CycH's spectra contain more exchanges but weaker peaks (Figure 2B, C), indicating more exchanges among states with the same *cis*−*trans* amide backbone. Collectively, we conclude that CycA and ALI populate more conformers with unique *cis*−*trans* amides in comparison to CycH, which could be important for membrane permeation. More importantly, the results suggest that exchanges among states captured by 2D-NMR can infer the conformational heterogeneity of cyclosporines. To illustrate the assumption that a cyclosporine characterized by low conformational heterogeneity (few conformers with distinct *cis*−*trans* amides) can exhibit numerous states (with the same *cis*−*trans* amides but differing backbone shapes or side chain orientations) and transitions between these states (as observed in the NMR data, Figure 2C), we calculated the RMSDs for the **C1** and **O1** conformers of CycA, ALI, and CycH. We chose these two conformers because all three macrocycles populate them. The RMSDs to the X-ray crystal structure for CycH's **C1** and **O1** display higher values and significantly broader ranges than those for CycA and ALI (Figure S5). This highlights that the conformers of CycA and ALI are more stable than that of CycH, exhibiting fewer variations in backbone structures and side chain orientations.

The IMS-MS data also support the conclusion from NMR (Figure 4). Of note, CycA and CycH were previously studied by Hyung et al. using traveling-wave IMS (TW-IMS), in which the ATD of CycA shows two features while that of CycH only shows one.[61] Our DT-IMS-MS data also support that CycH adopts fewer conformers than CycA, as the width of its IM profile is more narrow (Figure S6). Here, using cIMS-MS, which offers higher IM resolution than DT-IMS and TW-IMS, the difference in conformational heterogeneity of CycA and CycH is validated. The results from conformationally selected ion activation experiments validate that the CycH conformers are much less stable than CycA and ALI conformers.

Another line of compelling evidence is from our computational modeling data, where **O1** was found to be dominant in the conformation space of CycH (Figure 5). CycA and ALI, which have good membrane permeabilities, populated **A1** and **C1**. Also, from the computational data, the population of **A1** is significant for both CycA and ALI, indicating that it is crucial for membrane permeability. Intermediate conformers, some serendipitously captured in previous NMR experiments with salts,[55,62] are also detected in our simulations and experiments, as elaborated in the previous sections. While it is not yet possible to elucidate the specific role of these "rare" conformers, we particularly focused on the **I** conformer, which has two *cis*-amides Sar3—MeLeu4 and MeLeu9—MeLeu10. This conformer becomes visible in the presence of $CaCl_2$.

Calcium Chloride Promotes Low-Abundance Conformers

Because metal cations such as Na^+, K^+, Ca^{2+}, Mg^{2+}, or Zn^{2+} are found in biology at relatively high concentrations, they are essential and may contribute to the biochemistry of cyclosporines *in vivo*. However, their possible roles in the conformational isomerism of cyclosporines have not been fully investigated. The use of salts in NMR and X-ray crystallography experiments is precedented. For example, $Mg(ClO_4)_2$ was used to obtain X-ray crystal structures of free CycH and CycG.[33] KCl and NaCl can be used to crystallize the aqueous conformer (**A1**) of CycA.[28] In these crystallography experiments, no metal cations or counterions were found in the refined crystal structures, indicating that they do not bind strongly to the macrocycles and alter their structures. Their role was hypothesized to be involved in stabilizing flexible side chains such as MeBmt1.[33]

In parallel, a more diverse set of salts (and counterions) were used in early NMR experiments where uncommon *cis*-amide bonds of CycA were observed.[43,54,55,62,63] We previously showed that $CaCl_2$ greatly increased the population of CycA's **O1** in acetonitrile (that is otherwise a minor conformer), and Ca^{2+} was predicted to bind to CycA near D-Ala8 of **O1**.[54,62]

Our NMR and cIMS-MS data on CycA in the presence of $CaCl_2$ show the presence of the **I** conformer. Its presence is positively correlated with the increase in **O1** and the decrease in **A1**, suggesting that they could be important "catalytically" for the transition from **A1** (the aqueous conformer) to **O1** (the conformer required for binding the protein targets). However, as the mobility-selected cIMS-MS experiments (Figure 4C) indicate, $CaCl_2$ lowers the energy barriers for interconversion between **A1**, **O1**, and **C1**.

IRMPD spectroscopy of $[CycA+Ca]^{2+}$ shows that the presence of some CycA conformers is validated through the bands in the O−H/N-H stretching frequency region (Figure 6). The O−H/N-H stretching region varies slightly between conformers, as indicated by the DFT-calculated IR spectra in Figure 6B. Comparing this region of the calculated data to the experimental IRMPD data, it can be deduced that the $[CycA+Ca]^{2+}$ ion consists of **O1**, as indicated by a strong band at 3450 cm^{-1}, and possibly a mixture of **A1**, **C1**, and **I1** as indicated by a medium band at ∼3350 cm^{-1} and a very weak band near 3700 cm^{-1} (which is not predicted for **O1**). Notably, the IRMPD spectrum of peak **A1** (Figure 6B) closely resembles the calculated IR spectrum of **A1**. We hypothesize that some collisional activation occurs upon exiting the TIMS

https://doi.org/10.1021/jacsau.4c00011
JACS Au 2024, 4, 1458−1470

(i.e., MPE) and note the relatively long storage time in the ICR cell; the additional energy or prolonged storage time would allow for the conformational interconversion of the mobility-selected conformers to the original (no TIMS) conformational distribution. This is reminiscent of the re-established conformational ensembles observed in the cIMS data after the addition of activation voltage (Figure 4A). Nonetheless, the IRMPD data support the idea that **O1** is promoted by $CaCl_2$.

Here, we offer an explanation of the role of $CaCl_2$: The presence of salt can alter the dielectric properties of the solvent, causing a disturbance in the conformational ensemble. In simpler terms, $CaCl_2$ does not necessarily create a new conformation, but it renders otherwise less prevalent conformations detectable. Additionally, each salt has the potential to influence the peptide structure, introducing novel states.

It has been shown theoretically and experimentally that the addition of alkali and alkaline-earth halides to high dielectric solutions results in a nonlinear decrease in the dielectric constant due to ion-solvation effects.[64−68] Barthel and co-workers demonstrated the effects of various electrolytes on the dielectric constant and relaxation of acetonitrile by analyzing the complex permittivity spectra in the frequency range $0.95 \leq \nu$ (GHz) ≤ 89 at 25 °C.[69] The dielectric constants of the acetonitrile:electrolyte solutions, up to molarities of 1 M, were found to decrease regardless of the electrolyte identity.

Previous NMR data indicate that the closed conformer (**C1**) exists at 55% in deuterated acetonitrile compared to 19% in deuterated methanol/water.[54] **C1** is the most dominant conformer in a low-dielectric environment, while **O1** favors a high-dielectric, aqueous environment. Perhaps the presence of $CaCl_2$ at 5 mM lowers the dielectric constant of the acetonitrile (pure acetonitrile; $\varepsilon_s = 35.84$[69]) to slightly mimic the properties of methanol (pure methanol; $\varepsilon_s = 33.70$[70]) enough to alter the stability of **A1** and **O1**, but not **C1**. Note that $LiClO_4$ has been shown to increase the originally low dielectric constant of THF.[71] This further highlights the effects that metal cations have on the dielectric constant of the solvent, which is important for the solubility (stability) of the CycA conformers. What conformers would become visible may depend on the ability of the salt to alter solvent properties.

Of note, Köck et al. performed NMR on CycA in the presence of LiCl in deuterated tetrahydrofuran (THF).[63] They showed that CycA adopts **O1**, compared to only **C1** in the absence of LiCl. This means that the Li^+ and the Ca^{2+} ions have similar effects on the *cis/trans* amide preference of CycA. Gray et al.[54] compared the NMR chemical shifts of the all-*trans* conformers (**O**) observed in samples containing $CaCl_2$, LiCl, or CypA.[63] Variations in chemical shifts were noted, indicating that the salts may slightly modulate the structures of the conformer. An average difference of 0.52 ppm was observed for the backbone ^{1}H chemical shifts (Hα's and HN/MeN's).

This rationale could also provide support for earlier observations of atypical *cis*-amides when salts are present. For example, *cis* Sar3—MeLeu4 was observed in the presence of $CaCl_2$ (this work), $Mg(ClO_4)_2$,[55] and $Ca(ClO_4)_2$.[62] *Cis* Val5—MeLeu6 was observed in pure MeOD/H_2O,[28] or in the presence of $Ce(ClO_4)_3$.[55] *Cis* Abu2—Sar3 was also observed in pure MeOD/H_2O,[28] or in bound state of CycA to RGG.[27]

Furthermore, employing the cIMS platform, we conducted tandem MS/MS on mobility-selected $[CycA+Ca]^{2+}$ ions (Figure S8). Regrettably, the MS/MS spectra exhibited considerable similarity. This result can likely be attributed to the selected conformers undergoing equilibration into an ensemble during the collision-induced dissociation process.

Nonetheless, to further support our rationale that different salts may produce different states of the same conformer, we discuss the various states of **I** under different solvent conditions. With $CaCl_2$, we observed **I2**, which was visible at temperatures greater than 25 °C (Figure 3). **I2** has distinct chemical shifts from **C1,** and thus its chemical shifts can be fully assigned (Table S4). **I2** is also characterized by two hydrogen bonds between Abu2 and Val5 and between Ala7 and MeVal11.

Regarding **I*** observed in the NMR studies by Bernardi et al., who worked with $Mg(ClO_4)_2$,[55] that study reported very limited chemical shifts (mainly some Hαs). Therefore, we conducted NMR experiments on CycA with $Mg(ClO_4)_2$ to elucidate **I***. We found that the NMR chemical shifts of **I*** are different compared to the chemical shifts of **I2**; see Table S4. On average, a difference of 0.42 ppm was observed for the backbone ^{1}H chemical shifts (Hα's and HN/MeN's).

Regarding the atomistic structures, the structure obtained through the Mg^{2+}-restrained MD (**I***) by Bernardi coordinates Mg^{2+} inside the ring.[55] Our **I1** structure predicted by T-REMD (no salt) adopts a configuration comparable to **C1**,[56] with a small change in secondary structure at the novel *cis*-amide linkage. Thus, we expect the NMR chemical shifts of **I1** to largely overlap those of **C1**. In **C1**, the geometry around the Sar3-MeLeu4 peptide linkage adopts a standard type-II' β turn, characterized by an Abu2-NH···Val5-CO hydrogen bond. The predicted **I1** structure utilizes the same hydrogen bond to adopt instead a Type-VIb β turn ($\varphi-\psi$ angles given in Table S23), usually reserved for *cis*-proline bonds.[72] Comparing **C1** and **I1**, Abu2, Val5, and MeLeu6 differ only by rotamers likely to be in fast exchange at room temperature (Figure 7A, B).

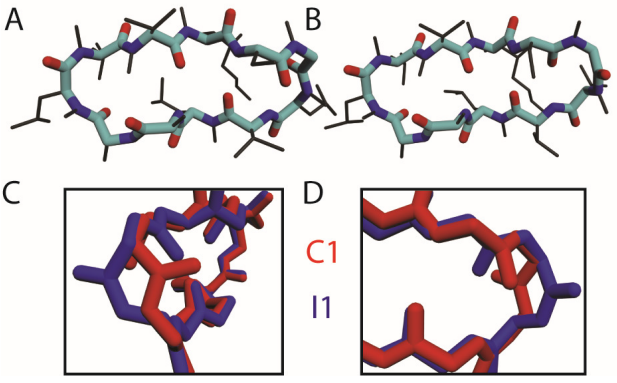

Figure 7. Comparison of backbone structures of (A) **C1** by Loosli et al.[29] and (B) **I1** obtained from T-REMD and optimized with B3LYP/def2svp, the D3 version of Grimme's empirical dispersion model, and using a self-consistent reaction field methanol solvent model. Side chain carbons are colored black to emphasize slight rotamer variation. The difference in the secondary structure around the Sar3—MeLeu4 peptide linkage is emphasized by both (C) front and (D) back views.

The backbone structure is identical aside from the β-turn region, and consequently, the hydrogen bonding of amide hydrogens distal to Sar3 and MeLeu4 is also identical to **C1**. The *cis*-amide linkage causes a deviation from the original Type II' secondary structure characteristic where the carbonyl appears on the other side of the plane of the macrocycle, giving

https://doi.org/10.1021/jacsau.4c00011
JACS Au 2024, 4, 1458−1470

a mirrored appearance relative to the **C1** closed form (Figure 7C, D). This finding is further validated by comparing **I*** and **C1** ^{1}H NMR chemical shifts. The chemical shifts of **I*** and **C1** are almost identical. Therefore, based on the consistent hydrogen bonding, *cis*-amide patterns, and chemical shift comparisons, we conclude that the **I*** conformer detected in the NMR experiments with $Mg(ClO_4)_2$ has the same structure as the one captured by the T-REMD simulation (i.e., **I*** = **I1**).

From T-REMD data and energy calculations, **I1** is one of the most favored structures of CycA, as it has the second lowest relative energy among all of the conformers of CycA, slightly less stable than **C1** but more stable than both **A1** and **O1**. We suspect that **I1** is always present at very low concentrations, but its detection by NMR requires higher temperatures in combination with the stability effects of the metal salts. **I2** is a result of **I1** being perturbed by $CaCl_2$, whereas $Mg(ClO_4)_2$ promoted and also retained **I1**. These salts can interact weakly with the macrocycle, change the ion−solvent pairing, and increase the dielectric constant of the environment. It would be valuable for future research to explore the effects of the counterions (the Hofmeister series) on the population of cyclosporine conformers.

Moreover, in the cIMS-MS data (Figure 4C), **I2** likely contributes to the broad tailing feature assigned to C1. Additionally, due to its β-turn structure, **I1**/**I2** are likely to be more abundant in low dielectric environments, suggesting its potential contribution to membrane permeation. This speculation finds support in the detection of *cis* Sar3—MeLeu4 in [CS−NH^{MeBmt}]CycA, which is a thiocyclosporin derivative of CycA where the C═O of MeBmt is replaced with C═S.[73]

Nonetheless, despite its higher energetic stability, the lower abundance of **I1** compared to that of **A1** and **O1** presents intriguing questions. The energy difference of 1.4 kcal/mol corresponds to a ratio of approximately 10:1. Considering that **I1** is approximately 5 kcal/mol higher in energy than **C1** (see Figure S3), it suggests that the abundance of **I1** (or **A1** and **O1**) should be negligible in comparison to that of **C1**. The role of **I1**/**I2** and whether the high *cis* propensity of Sar3 and MeLeu4 impacts the activity of CycA remains unclear. In membrane-permeable ALI, **I1** is reduced and replaced by a conformer with *cis* Val5—MeLeu6 and MeVal11—MeBmt1. In future research, it would be valuable to investigate the effects of enforcing *trans* configurations for Sar3—MeLeu4 and Val5—MeLeu6 to determine whether the activity of cyclosporines is compromised.

Then why are **O1** and **A1** observed? The all-*trans* **O1** conformer represents a transitional state between conformers with distinct *cis*-amides. In the presence of metal salts, the conformational population distribution can be altered, changing the relative abundance of the conformers that are already in solution, such as leading to a higher occurrence of **O1** despite its higher energy level. Lastly, **A1** demonstrates the capability to engage in hydrogen bonding with water,[28] which significantly contributes to its stability and may account for its higher abundance compared to **I1**.

CONCLUSION

Our study reveals that access to the **A1** conformer, not the **O1** conformer, facilitates membrane permeation of cyclosporines. When the **C1** conformer is excessively stable, it may become trapped or immobilized within the membrane, hindering its functionality. While **C1** is more populated in low-dielectric environments (such as a membrane), it is not enough to make the macrocycle membrane-permeable. Membrane permeability is likely driven by the transitions between **C1** and **A1**. Further studies will investigate into the intermediates between the two conformers, especially at the interface between aqueous and membrane. Moreover, **O1** is populated only in the presence of $CaCl_2$.

Metal salts such as $CaCl_2$ perturb conformational population distributions, leading to increased visibility of low-abundance, high-energy conformers. We suggest that these conformers are responsive to the dielectric properties of the environment, potentially influencing their solubility (or stability). Our investigation uncovered up to four major conformers of CycA in solution, highlighting the intricate interplay between conformers with known and unknown functions.

Significantly, the impact of metal cations primarily involves modification of solvent dielectric properties and conformer stability rather than specific chelation to particular residues. Although these nuanced effects have been discerned through crystallography, their thorough investigation necessitates the integration of various techniques, such as gas-phase ion mobility spectrometry, spectroscopy, solution-phase NMR, and computational modeling, as exemplified in the present study.

Moreover, this work addresses the incomplete passive membrane permeability hypothesis, which previously focused solely on the **C1** and **O1** conformers.[19,74,75] It also helps reconcile conflicting data regarding the structure−function relationship of cyclosporines, putting more spotlight on the aqueous conformers of cyclosporines. The positive correlation between the presence of "rare" conformers with unique *cis*-amides, such as **I1** and **I2**, and the transition from **A1** to **O1** may indicate the roles of "redundant" *N*-methylation found in cyclosporines. The access to their high-energy conformers increases the chance for the macrocycles to adapt to the untraditional protein binding sites. It also allows for a more fluid transition among chemical environments, such as membranes and aqueous. Our study provides the fundamental principles that will aid the design of future large cyclic peptides for intracellular targets.

Finally, through the concurrent application of solution-phase (NMR) and gas-phase (IMS-MS and IRMPD) analyses on cyclosporines, we demonstrated that gas-phase methods are effective at preserving the conformers observed in the solution phase and exhibit good predictive power in identifying novel conformers. This comprehensive approach allows us to capture not only the lowest-energy conformers (e.g., **C1** of CycA) but also higher-energy conformers (**A1** and **O1**) and minor conformers (**I2**) that bear relevance to the biochemical properties of the macrocycle. Our investigation also underscored challenges in acquiring structural data of macrocyclic peptide conformers, considering that energy barriers for interconversion can often be modulated through ion activation, trapping, and laser irradiation. Additionally, we suggest that softer methods, such as cryogenic MS, may be able to address these challenges.

ASSOCIATED CONTENT

Supporting Information

The Supporting Information is available free of charge at https://pubs.acs.org/doi/10.1021/jacsau.4c00011.

https://doi.org/10.1021/jacsau.4c00011
JACS Au 2024, 4, 1458−1470

Detailed experimental methods and instrument parameters (Tables S1−S3), NMR chemical shift assignments (Tables S4−S15), NMR hydrogen bond calculations (Tables S16−S21), AMBER parameters (Table 22), theoretical CCS values (Table S23), angles of β-turns in CycA conformers (Table S24), block analysis and convergence test for REMD simulations (Figure S1), correlation matrices obtained from REMD data (Figure S2), DFT data (Figure S3), and additional IMS-MS, REMD, and NMR data (Figures S4−S9) (PDF)

AUTHOR INFORMATION

Corresponding Author

Thanh D. Do − *Department of Chemistry, University of Tennessee, Knoxville, Tennessee 37996, United States;* orcid.org/0000-0002-1978-4365; Email: tdo5@tennessee.edu

Authors

Miranda N. Limbach − *Department of Chemistry, University of Tennessee, Knoxville, Tennessee 37996, United States;* orcid.org/0000-0003-4266-7279

Edward T. Lindberg − *Department of Chemistry, University of Tennessee, Knoxville, Tennessee 37996, United States*

Hernando J. Olivos − *Waters Corporation, Milford, Massachusetts 01757, United States*

Lara van Tetering − *Institute for Molecules and Materials, FELIX Laboratory, Radboud University, Nijmegen 6525 ED, The Netherlands;* orcid.org/0009-0003-5070-6116

Carlos A. Steren − *Department of Chemistry, University of Tennessee, Knoxville, Tennessee 37996, United States;* orcid.org/0000-0002-0455-4137

Jonathan Martens − *Institute for Molecules and Materials, FELIX Laboratory, Radboud University, Nijmegen 6525 ED, The Netherlands;* orcid.org/0000-0001-9537-4117

Van A. Ngo − *Advanced Computing for Life Sciences and Engineering Group, Science Engagement Section, National Center for Computational Sciences, Computing and Computational Sciences Directorate, Oak Ridge National Laboratory, Oak Ridge, Tennessee 37830, United States;* orcid.org/0000-0001-8350-1203

Jos Oomens − *Institute for Molecules and Materials, FELIX Laboratory, Radboud University, Nijmegen 6525 ED, The Netherlands*

Complete contact information is available at: https://pubs.acs.org/10.1021/jacsau.4c00011

Author Contributions

T.D.D. conceived and managed the project. M.N.L. collected the DT-IMS and 2D-NMR data. E.T.L. performed and analyzed REMD simulations. L.v.T., J.M., and J.O. performed the IRMPD experiments. H.J.O. collected the cIMS-MS data. T.D.D., M.L.N., E.T.L., C.A.S., V.A.N., and J.O. designed the experiments. The manuscript was written through the contributions of all authors. All authors have given approval to the final version of the manuscript. CRediT:**Miranda N. Limbach** formal analysis, investigation, methodology, writing-original draft, writing-review & editing; **Edward Lindberg** formal analysis, investigation, writing-original draft, writing-review & editing; **Hernando J. Olivos** data curation, investigation, methodology; **Lara van Tetering** formal analysis, investigation, writing-review & editing; **Carlos A. Steren** methodology, writing-review & editing; **Jonathan Martens** formal analysis, investigation; **Van A. Ngo** methodology, resources, writing-review & editing; **Jos Oomens** data curation, formal analysis, investigation, methodology, project administration, resources, supervision, writing-review & editing; **Thanh D Do** conceptualization, formal analysis, funding acquisition, investigation, methodology, project administration, resources, supervision, writing-original draft, writing-review & editing.

Funding

Eli Lily and Co. Young Investigator Award (to T.D.D.).

Notes

The authors declare no competing financial interest.

ACKNOWLEDGMENTS

Alisoporivir (ALI) used in this work was generously donated to us by Debiopharm. We thank Nathalie Favre for the support. We also thank Dr. Michael Best for helpful discussion. This research used resources (project number CHM188 to T.D.D.) of the Oak Ridge Leadership Computing Facility, which is a DOE Office of Science User Facility supported under Contract DE-AC05-00OR22725. This work used Expanse and Expanse GPU at San Diego Supercomputer Center through allocation BIO220150 (to T.D.D.) from the Advanced Cyberinfrastructure Coordination Ecosystem: Services & Support (ACCESS) program, which is supported by National Science Foundation grants #2138259, #2138286, #2138307, #2137603, and #2138296. This work was supported by HFML-RU, a member of the European Magnetic Field Laboratory (EMFL).

REFERENCES

(1) Lipinski, C. A.; Lombardo, F.; Dominy, B. W.; Feeney, P. J. Experimental and computational approaches to estimate solubility and permeability in drug discovery and development settings. *Adv. Drug Delivery Rev.* **2001**, *46*, 3−26.

(2) Lipinski, C. A. Lead- and drug-like compounds: the rule-of-five revolution. *Drug Discovery Today Technol.* **2004**, *1*, 337−341.

(3) Leeson, P. D.; Springthorpe, B. The influence of drug-like concepts on decision-making in medicinal chemistry. *Nat. Rev. Drug Discovery* **2007**, *6*, 881−890.

(4) Driggers, E. M.; Hale, S. P.; Lee, J.; Terrett, N. K. The exploration of macrocycles for drug discovery — an underexploited structural class. *Nat. Rev. Drug Discovery* **2008**, *7*, 608−624.

(5) Mallinson, J.; Collins, I. Macrocycles in new drug discovery. *Future Med. Chem.* **2012**, *4*, 1409−1438.

(6) Marsault, E.; Peterson, M. L. Macrocycles are great cycles: applications, opportunities, and challenges of synthetic macrocycles in drug discovery. *J. Med. Chem.* **2011**, *54*, 1961−2004.

(7) Wu, W. H.; Guo, J. W.; Zhang, L. S.; Zhang, W. B.; Gao, W. P. Peptide/protein-based macrocycles: from biological synthesis to biomedical applications. *RSC Chem. Biol.* **2022**, *3*, 815−829.

(8) Yudin, A. K. Macrocycles: lessons from the distant past, recent developments, and future directions. *Chem. Sci.* **2015**, *6*, 30−49.

(9) Verdine, G. L.; Walensky, L. D. The challenge of drugging undruggable targets in cancer: lessons learned from targeting BCL-2 family members. *Clin. Cancer Res.* **2007**, *13*, 7264−7270.

(10) Dang, C. V.; Reddy, E. P.; Shokat, K. M.; Soucek, L. Drugging the 'undruggable' cancer targets. *Nat. Rev. Cancer* **2017**, *17*, 502−508.

(11) Zhang, G.; Zhang, J.; Gao, Y.; Li, Y.; Li, Y. Strategies for targeting undruggable targets. *Expert Opin. Drug Discovery* **2022**, *17*, 55−69.

(12) Mullard, A. 2021 FDA approvals. *Nat. Rev. Drug Discovery* **2022**, *21*, 83−89.

(13) Zhang, H.; Chen, S. Cyclic peptide drugs approved in the last two decades (2001−2021). *RSC Chem. Biol.* **2022**, *3*, 18−31.
(14) Costa, L.; Sousa, E.; Fernandes, C. Cyclic Peptides in Pipeline: What Future for These Great Molecules? *Pharmaceuticals* **2023**, *16*, 996.
(15) Benedetto Tiz, D.; Bagnoli, L.; Rosati, O.; Marini, F.; Santi, C.; Sancineto, L. FDA-Approved Small Molecules in 2022: Clinical Uses and Their Synthesis. *Pharmaceutics* **2022**, *14*, 2538.
(16) Patocka, J.; Nepovimova, E.; Kuca, K.; Wu, W. D. Cyclosporine A: Chemistry and Toxicity - A Review. *Curr. Med. Chem.* **2021**, *28*, 3925−3934.
(17) Tedesco, D.; Haragsim, L. Cyclosporine: a review. *J. Transplant.* **2012**, *2012*, 230386.
(18) Zenke, G.; Baumann, G.; Wenger, R.; Hiestand, P.; Quesniaux, V.; Andersen, E.; Schreier, M. H. Molecular Mechanisms of Immunosuppression by Cyclosporins. *Ann. N.Y. Acad. Sci.* **1993**, *685*, 330−335.
(19) Ahlbach, C. L.; Lexa, K. W.; Bockus, A. T.; Chen, V.; Crews, P.; Jacobson, M. P.; Lokey, R. S. Beyond cyclosporine A: conformation-dependent passive membrane permeabilities of cyclic peptide natural products. *Future Med. Chem.* **2015**, *7*, 2121−2130.
(20) Corbett, K. M.; Ford, L.; Warren, D. B.; Pouton, C. W.; Chalmers, D. K. Cyclosporin Structure and Permeability: From A to Z and Beyond. *J. Med. Chem.* **2021**, *64*, 13131−13151.
(21) Lee, D.; Lee, S.; Choi, J.; Song, Y.-K.; Kim, M. J.; Shin, D.-S.; Bae, M. A.; Kim, Y.-C.; Park, C.-J.; Lee, K.-R.; Choi, J.-H.; Seo, J. Interplay among Conformation, Intramolecular Hydrogen Bonds, and Chameleonicity in the Membrane Permeability and Cyclophilin A Binding of Macrocyclic Peptide Cyclosporin O Derivatives. *J. Med. Chem.* **2021**, *64*, 8272−8286.
(22) Loor, F.; Tiberghien, F.; Wenandy, T.; Didier, A.; Traber, R. Cyclosporins: structure-activity relationships for the inhibition of the human MDR1 P-glycoprotein ABC transporter. *J. Med. Chem.* **2002**, *45*, 4598−4612.
(23) Loor, F.; Tiberghien, F.; Wenandy, T.; Didier, A.; Traber, R. Cyclosporins: structure-activity relationships for the inhibition of the human FPR1 formylpeptide receptor. *J. Med. Chem.* **2002**, *45*, 4613−4628.
(24) Kallen, J.; Spitzfaden, C.; Zurini, M. G.; Wider, G.; Widmer, H.; Wuthrich, K.; Walkinshaw, M. D. Structure of human cyclophilin and its binding site for cyclosporin A determined by X-ray crystallography and NMR spectroscopy. *Nature* **1991**, *353*, 276−279.
(25) Mikol, V.; Kallen, J.; Pflugl, G.; Walkinshaw, M. D. X-ray structure of a monomeric cyclophilin A-cyclosporin A crystal complex at 2.1 A resolution. *J. Mol. Biol.* **1993**, *234*, 1119−1130.
(26) Weber, C.; Wider, G.; von Freyberg, B.; Traber, R.; Braun, W.; Widmer, H.; Wuthrich, K. The NMR structure of cyclosporin A bound to cyclophilin in aqueous solution. *Biochem.* **1991**, *30*, 6563−6574.
(27) Parashar, V.; Aggarwal, C.; Federle, M. J.; Neiditch, M. B. Rgg protein structure-function and inhibition by cyclic peptide compounds. *Proc. Natl. Acad. Sci. U. S. A.* **2015**, *112*, 5177−5182.
(28) Limbach, M. N.; Antevska, A.; Oluwatoba, D. S.; Gray, A. L. H.; Carroll, X. B.; Hoffmann, C. M.; Wang, X.; Voehler, M.; Steren, C. A.; Do, T. D. Atomic View of Aqueous Cyclosporine A: Unpacking a Decades-Old Mystery. *J. Am. Chem. Soc.* **2022**, *144*, 12602−12607.
(29) Loosli, H.-R.; Kessler, H.; Oschkinat, H.; Weber, H.-P.; Petcher, T. J.; Widmer, A. Peptide conformations. Part 31. The conformation of cyclosporin A in the crystal and in solution. *Helv. Chim. Acta* **1985**, *68*, 682−704.
(30) Rüdisser, S. H.; Matabaro, E.; Sonderegger, L.; Güntert, P.; Künzler, M.; Gossert, A. D. Conformations of Macrocyclic Peptides Sampled by Nuclear Magnetic Resonance: Models for Cell-Permeability. *J. Am. Chem. Soc.* **2023**, *145*, 27601.
(31) Burdmann, E. A.; Andoh, T. F.; Rosen, S.; Lindsley, J.; Munar, M. Y.; Elzinga, L. W.; Bennett, W. M. Experimental nephrotoxicity, hepatotoxicity and pharmacokinetics of cyclosporin G versus cyclosporin A. *Kidney Int.* **1994**, *45*, 684−691.
(32) Hoyt, E. G.; Hagberg, C.; Billingham, M. E.; Baldwin, J. C.; Jamieson, S. W. Analysis of the immunosuppressive and nephrotoxic effects of cyclosporin G. *J. Heart Transplant.* **1988**, *7*, 111−117.
(33) Potter, B.; Palmer, R. A.; Withnall, R.; Jenkins, T. C.; Chowdhry, R. Z. Two new cyclosporin folds observed in the structures of the immunosuppressant cyclosporin G and the formyl peptide receptor antagonist cyclosporin H at ultra-high resolution. *Org. Biomol. Chem.* **2003**, *1*, 1466−1474.
(34) dePaulis, A.; Ciccarelli, A.; deCrescenzo, G.; Cirillo, R.; Patella, V.; Marone, G. Cyclosporin H is a potent and selective competitive antagonist of human basophil activation by N-formyl-methionyl-leucyl-phenylalanine. *J. Allergy Clin. Immunol.* **1996**, *98*, 152−164.
(35) Quarato, G.; D'Aprile, A.; Gavillet, B.; Vuagniaux, G.; Moradpour, D.; Capitanio, N.; Piccoli, C. The cyclophilin inhibitor alisporivir prevents hepatitis C virus-mediated mitochondrial dysfunction. *Hepatol.* **2012**, *55*, 1333−1343.
(36) Landrieu, I.; Hanoulle, X.; Fritzinger, B.; Horvath, D.; Wieruszeski, J. M.; Lippens, G. Ranking High Affinity Ligands of Low Solubility by NMR Spectroscopy. *ACS Med. Chem. Lett.* **2011**, *2*, 485−487.
(37) Dujardin, M.; Bouckaert, J.; Rucktooa, P.; Hanoulle, X. X-ray structure of alisporivir in complex with cyclophilin A at 1.5 angstrom resolution. *Acta Crystallogr. Sect. F Struct. Biol. Comm.* **2018**, *74*, 583−592.
(38) Ptak, R. G.; Gallay, P. A.; Jochmans, D.; Halestrap, A. P.; Ruegg, U. T.; Pallansch, L. A.; Bobardt, M. D.; de Bethune, M. P.; Neyts, J.; De Clercq, E.; Dumont, J. M.; Scalfaro, P.; Besseghir, K.; Wenger, R. M.; Rosenwirth, B. Inhibition of human immunodeficiency virus type 1 replication in human cells by Debio-025, a novel cyclophilin binding agent. *Antimicrob. Agents Chemother.* **2008**, *52*, 1302−1317.
(39) Coelmont, L.; Kaptein, S.; Paeshuyse, J.; Vliegen, I.; Dumont, J. M.; Vuagniaux, G.; Neyts, J. Debio 025, a Cyclophilin Binding Molecule, Is Highly Efficient in Clearing Hepatitis C Virus (HCV) Replicon-Containing Cells When Used Alone or in Combination with Specifically Targeted Antiviral Therapy for HCV (STAT-C) Inhibitors. *Antimicrob. Agents Chemother.* **2009**, *53*, 967−976.
(40) Paeshuyse, J.; Kaul, A.; De Clercq, E.; Rosenwirth, B.; Dumont, J. M.; Scalfaro, P.; Bartenschlager, R.; Neyts, J. The non-immunosuppressive cyclosporin DEBIO-025 is a potent inhibitor of hepatitis C virus replication in vitro. *Hepatol.* **2006**, *43*, 761−770.
(41) Softic, L.; Brillet, R.; Berry, F.; Ahnou, N.; Nevers, Q.; Morin-Dewaele, M.; Hamadat, S.; Bruscella, P.; Fourati, S.; Pawlotsky, J. M.; Ahmed-Belkacem, A. Inhibition of SARS-CoV-2 Infection by the Cyclophilin Inhibitor Alisporivir (Debio 025). *Antimicrob. Agents Chemother.* **2020**, *64*, No. e00876-20.
(42) Efimov, S.; Zgadzay, Y.; Klochkov, V. Observation of Conformational Exchange in Cyclosporin in Media of Varying Polarity by NMR Spectroscopy. *Appl. Magn. Reson.* **2014**, *45*, 1225−1235.
(43) Kofron, J. L.; Kuzmic, P.; Kishore, V.; Gemmecker, G.; Fesik, S. W.; Rich, D. H. Lithium-Chloride Perturbation of Cis-Trans Peptide-Bond Equilibria - Effect on Conformational Equilibria in Cyclosporine-a and on Time-Dependent Inhibition of Cyclophilin. *J. Am. Chem. Soc.* **1992**, *114*, 2670−2675.
(44) Ujma, J.; Ropartz, D.; Giles, K.; Richardson, K.; Langridge, D.; Wildgoose, J.; Green, M.; Pringle, S. Cyclic Ion Mobility Mass Spectrometry Distinguishes Anomers and Open-Ring Forms of Pentasaccharides. *J. Am. Soc. Mass Spectrom.* **2019**, *30*, 1028−1037.
(45) Oomens, J.; Sartakov, B. G.; Meijer, G.; von Helden, G. Gas-phase infrared multiple photon dissociation spectroscopy of mass-selected molecular ions. *Int. J. Mass. Spectrom.* **2006**, *254*, 1−19.
(46) Maitre, P.; Scuderi, D.; Corinti, D.; Chiavarino, B.; Crestoni, M. E.; Fornarini, S. Applications of Infrared Multiple Photon Dissociation (IRMPD) to the Detection of Posttranslational Modifications. *Chem. Rev.* **2020**, *120*, 3261−3295.
(47) Polfer, N. C. Infrared multiple photon dissociation spectroscopy of trapped ions. *Chem. Soc. Rev.* **2011**, *40*, 2211−2221.

https://doi.org/10.1021/jacsau.4c00011
JACS Au 2024, 4, 1458−1470

(48) Maier, J. A.; Martinez, C.; Kasavajhala, K.; Wickstrom, L.; Hauser, K. E.; Simmerling, C. ff14SB: Improving the Accuracy of Protein Side Chain and Backbone Parameters from ff99SB. *J. Chem. Theory Comput.* **2015**, *11*, 3696−3713.
(49) Vanquelef, E.; Simon, S.; Marquant, G.; Garcia, E.; Klimerak, G.; Delepine, J. C.; Cieplak, P.; Dupradeau, F.-Y. R.E.D. Server: a web service for deriving RESP and ESP charges and building force field libraries for new molecules and molecular fragments. *Nucleic Acids Res.* **2011**, *39*, W511−W517.
(50) Bayly, C. I.; Cieplak, P.; Cornell, W. D.; Kollman, P. A. A Well-Behaved Electrostatic Potential Based Method Using Charge Restraints for Deriving Atomic Charges - the Resp Model. *J. Phys. Chem.* **1993**, *97*, 10269−10280.
(51) Dupradeau, F. Y.; Pigache, A.; Zaffran, T.; Savineau, C.; Lelong, R.; Grivel, N.; Lelong, D.; Rosanski, W.; Cieplak, P. The R.ED. tools: advances in RESP and ESP charge derivation and force field library building. *Phys. Chem. Chem. Phys.* **2010**, *12*, 7821−7839.
(52) Vanquelef, E.; Simon, S.; Marquant, G.; Garcia, E.; Klimerak, G.; Delepine, J. C.; Cieplak, P.; Dupradeau, F. Y. RED Server: a web service for deriving RESP and ESP charges and building force field libraries for new molecules and molecular fragments. *Nucleic Acids Res.* **2011**, *39*, W511−W517.
(53) Wang, F.; Becker, J. P.; Cieplak, P.; Dupradeau, F. Y. RED Python: Object oriented programming for Amber force fields. *Abstracts of Papers of the American Chemical Society*; American Chemical Society, 2014; Vol. *247*.
(54) Gray, A. L. H.; Steren, C. A.; Haynes, I. W.; Bermejo, G. A.; Favretto, F.; Zweckstetter, M.; Do, T. D. Structural Flexibility of Cyclosporine A Is Mediated by Amide Cis-Trans Isomerization and the Chameleonic Roles of Calcium. *J. Phys. Chem. B* **2021**, *125*, 1378−1391.
(55) Bernardi, F.; Gaggelli, E.; Molteni, E.; Porciatti, E.; Valensin, D.; Valensin, G. H-1 and C-13-NMR and molecular dynamics studies of cyclosporin A interacting with magnesium(II) or cerium(III) in acetonitrile. Conformational changes and cis-trans conversion of peptide bonds. *Biophys. J.* **2006**, *90*, 1350−1361.
(56) Loosli, H.-R.; Kessler, H.; Oschkinat, H.; Weber, H.-P.; Petcher, T. J.; Widmer, A. Peptide Conformations. Part 31. The Conformation of Cyclosporin a in the Crystal and in Solution. *Helv. Chim. Acta* **1985**, *68*, 682−704.
(57) Jegorov, A.; Cvak, L.; Husek, A.; Šimek, P.; Heydová, A.; Ondráček, J.; Pakhomova, S.; Hušák, M.; Kratochvíl, B.; Sedmera, P.; Havlíček, V. Synthesis and Crystal Structure Determination of Cyclosporin H. *Collect. Czech. Chem. Commun.* **2000**, *65*, 1317−1328.
(58) Ono, S.; Naylor, M. R.; Townsend, C. E.; Okumura, C.; Okada, O.; Lee, H. W.; Lokey, R. S. Cyclosporin A: Conformational Complexity and Chameleonicity. *J. Chem. Inf. Model.* **2021**, *61*, 5601−5613.
(59) Houthuijs, K. J. Advancing molecular structure elucidation using infrared ion spectroscopy. *Dissertation*; Radboud University, Nijmegen, The Netherlands, 2023.
(60) Lee, D.; Choi, J.; Yang, M. J.; Park, C. J.; Seo, J. Controlling the Chameleonic Behavior and Membrane Permeability of Cyclosporine Derivatives via Backbone and Side Chain Modifications. *J. Med. Chem.* **2023**, *66*, 13189−13204.
(61) Hyung, S. J.; Feng, X. D.; Che, Y.; Stroh, J. G.; Shapiro, M. Detection of conformation types of cyclosporin retaining intramolecular hydrogen bonds by mass spectrometry. *Anal. Bioanal. Chem.* **2014**, *406*, 5785−5794.
(62) Carver, J. A.; Rees, N. H.; Turner, D. L.; Senior, S. J.; Chowdhry, B. Z. NMR-Studies of the Na+, Mg2+ and Ca2+ Complexes of Cyclosporine-A. *J. Chem. Soc., Chem. Commun.* **1992**, 1682−1684.
(63) Kock, M.; Kessler, H.; Seebach, D.; Thaler, A. Novel Backbone Conformation of Cyclosporine-a - the Complex with Lithium-Chloride. *J. Am. Chem. Soc.* **1992**, *114*, 2676−2686.
(64) Hasted, J. B.; Ritson, D. M.; Collie, C. H. Dielectric Properties of Aqueous Ionic Solutions 0.1.2. *J. Chem. Phys.* **1948**, *16*, 1−21.
(65) Levy, A.; Andelman, D.; Orland, H. Dielectric Constant of Ionic Solutions: A Field-Theory Approach. *Phys. Rev. Lett.* **2012**, *108*, 227801.
(66) Navarkhele, V. V.; Agrawal, R. S.; Kurtadikar, M. L. Dielectric properties of electrolytic solutions. *Pramana* **1998**, *51*, 511−518.
(67) Nortemann, K.; Hilland, J.; Kaatze, U. Dielectric properties of aqueous NaCl solutions at microwave frequencies. *J. Phys. Chem. A* **1997**, *101*, 6864−6869.
(68) Wei, Y. Z.; Chiang, P.; Sridhar, S. Ion Size Effects on the Dynamic and Static Dielectric-Properties of Aqueous Alkali Solutions. *J. Chem. Phys.* **1992**, *96*, 4569−4573.
(69) Barthel, J.; Kleebauer, M.; Buchner, R. Dielectric-Relaxation of Electrolyte-Solutions in Acetonitrile. *J. Solution Chem.* **1995**, *24*, 1−17.
(70) Jordan, B. P.; Sheppard, R. J.; Szwarnowski, S. Dielectric Properties of Formamide, Ethanediol and Methanol. *J. Phys. D: Appl. Phys.* **1978**, *11*, 695−701.
(71) Farber, H.; Petrucci, S. Ultrahigh Frequency and Microwave Relaxation of Lithium Perchlorate in Tetrahydrofuran. *J. Phys. Chem.* **1975**, *79*, 1221−1227.
(72) de Brevern, A. G. Extension of the classical classification of beta-turns. *Sci. Rep.* **2016**, *6*, 33191.
(73) Seebach, D.; Ko, S. Y.; Kessler, H.; Kock, M.; Reggelin, M.; Schmieder, P.; Walkinshaw, M. D.; Bolsterli, J. J.; Bevec, D. Thiocyclosporins - Preparation, Solution and Crystal-Structure, and Immunosuppressive Activity. *Helv. Chim. Acta* **1991**, *74*, 1953−1990.
(74) Wang, S. Z.; Witek, J.; Landrum, G. A.; Riniker, S. Improving Conformer Generation for Small Rings and Macrocycles Based on Distance Geometry and Experimental Torsional-Angle Preferences. *J. Chem. Inf. Model.* **2020**, *60*, 2044−2058.
(75) Witek, J.; Muhlbauer, M.; Keller, B. G.; Blatter, M.; Meissner, A.; Wagner, T.; Riniker, S. Interconversion Rates between Conformational States as Rationale for the Membrane Permeability of Cyclosporines. *ChemPhysChem* **2017**, *18*, 3309−3314.

https://doi.org/10.1021/jacsau.4c00011
JACS Au 2024, 4, 1458−1470